

Transport of biomolecules on compartmentalized membranes and its effect on reaction kinetics

Sumantra Sarkar

Center for Nonlinear Studies, Los Alamos National Laboratory

Well Mixed-Mass Action (WMMA) kinetics is widely used to model various reactions. However, the fundamental assumptions underlying WMMA kinetics are usually violated in biomolecular contexts. In this Letter we investigate the diffusive transport and diffusion mediated reactions of biomolecules on plasma membranes compartmentalized by the interaction of cortical actin and transmembrane proteins. In that context, we investigate the validity of WMMA kinetics for reactions occurring on the plasma membrane. We find that for most biologically relevant conditions WMMA kinetics is violated. We characterize the violation and investigate its origin.

The rate of every reaction is determined by two processes: (a) the transport of the molecules within reaction radius and (b) interaction of the molecules to form the products once they are closer than the reaction radius [1–4]. If the transport rate is k_D and the product formation rate is k_I , then the reaction rate r is given by:

$$r = k_D k_I / (k_D + k_I). \quad (1)$$

The dependence of k_D and k_I on the system parameters determine the reaction kinetics. Well Mixed-Mass Action (WMMA) kinetics is a widely used model of reaction kinetics in physical, chemical, and biological systems. Developed to describe the evolution of chemicals in solution [2], this principle posits that the rate of a reaction is proportional to the product of the reactant concentrations raised to a power equal to their stoichiometry. For example, for the dimerization reaction $S + S \rightleftharpoons S_2$, the reaction rate r is given by:

$$r = \kappa \times \frac{[S]([S] - 1)}{2} \quad (2)$$

$$= \kappa \times \phi, \quad (3)$$

where $n_S = [S]$ is the concentration of S , $\phi = [S]([S] - 1)/2$ is the mass-action flux, and κ is a proportionality factor. For WMMA kinetics, κ is a constant independent of the mass-action flux and is known as the *rate constant*. Well mixed (WM) kinetics assumes that transport of the molecules happen at a much faster rate than the rate of product formation, $k_D \gg k_I$, so that $r \approx k_I$ in Eqn. 1. On the other hand mass action (MA) kinetics assumes that the interaction of the reacting molecules happen purely through independent hard sphere collision processes, which leads to the kinetic law described in Eqn. 2.

In biological systems none of the assumptions underlying WMMA kinetics are usually satisfied. For example, for cell signaling systems, the concentration of the signaling molecules are in nM or μ M region. Bringing these molecules within reacting distance through diffusion, the main mode of transportation in biological systems, requires more than 1μ s, whereas the typical reaction times are often in ps to ns range. Therefore, the transport

processes are usually much slower than the product formation step [5, 6]. Hence the reaction rate $r \approx k_D$. Such *diffusion limited reactions* depend on the boundary conditions associated with the system and may lead to spatial patterns [7, 8], breaking down the well-mixed assumption. In addition, biomolecules interact with each other through complex interaction potentials. Rarely can these interactions be treated as hard collisions [2, 4]. Ostensibly, such complicated interactions lead to the breakdown of the mass-action assumption as well. Therefore, it is imperative to understand the validity of the WMMA kinetics for biomolecular systems and characterize its violation for biologically relevant boundary conditions.

Dimerization in picket enclosed compartments: In the so called *fence and pickets* model of the plasma membrane organization, the cytoskeletal actin near the plasma membrane, called cortical actin (*the fence*), attaches to the membrane and partitions it into submicron-sized compartments [9–13]. Some transmembrane proteins (*the pickets*) attach to the cortical actin fibers on the cytosolic side (inner leaflet) of the plasma membrane and forms barrier to free diffusion on the extracellular side (outer leaflet) of the plasma membrane [11](Fig. 1A-B). Since the pickets attach to the compartments created by the cortical actins, their arrangement on the outer-leaflet mimic the structure of the compartments. In this Letter, we study the kinetics of the dimerization reaction of a biomolecule S on such a *compartmentalized outer-leaflet of the plasma membrane*. It has been shown that confinement of the molecules within compartments change from constant rate of reactions to burst like activities as the permeability of the compartments is decreased [14]. However, in that study, the rate of confinement is chosen arbitrarily and no connection is made to the microscopic parameters, such as the density of the pickets, their sizes, and the size of the compartments. Furthermore, the confinement of the biomolecules in the inner-leaflet compartment leads to subdiffusive transport [9–11, 15]. Does the confinement by the pickets on the outer-leaflet also lead to subdiffusive behavior? How does the confinement affect diffusion limited dimerization of the biomolecules? To study these questions, we idealize the compartments

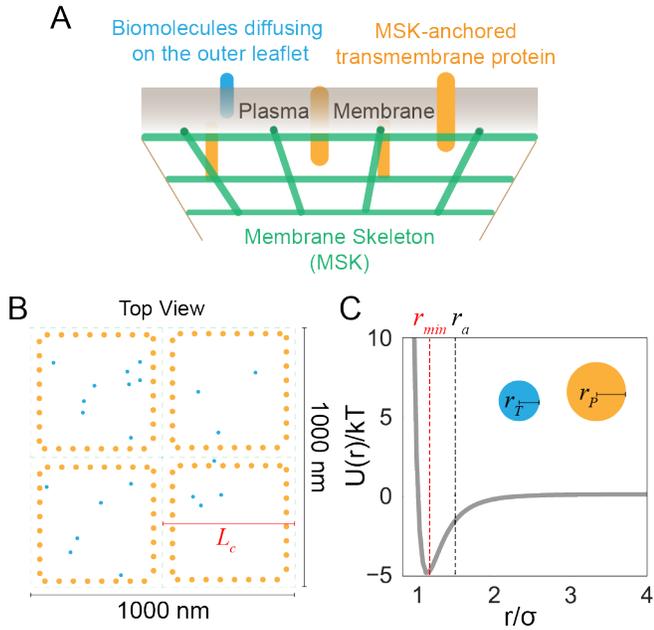


FIG. 1. Simulation details: (A) Pickets are membrane skeleton (green lines) anchored transmembrane proteins (orange) that produces compartment like structures on the outer leaflet of the plasma membranes [9]. We study the diffusion of small biomolecules (blue) on this structure using an idealized model. (B) Top view of the idealized model. We model the membrane as a 2D plane compartmentalized by immobilized pickets (orange disks) on which the biomolecules (blue disks) diffuse. A particular case with $n_C = 2/\mu\text{m}^2$ and $n_P = 16/\mu\text{m}^2$ is shown here. Compartment boundaries are indicated by green dashed lines. (C) The Lennard-Jones (LJ) interaction potential. We use both LJ and WCA interaction potential to model the interaction between the different biomolecules, pickets included. WCA interaction is first felt at $r_{\min} \equiv 2^{1/6}\sigma$, where $\sigma = r_T + r_P$. r_a is the reaction radius, the distance below which two molecules start reacting with each other.

formed by the cortical actin fence as a square lattice with lattice spacing L_c or, equivalently, with a compartment density $n_c = L_c^{-2}$. These compartments reside on a plasma membrane, which we model as a periodic 2D plane. The pickets are pinned molecules with identical radius r_P . They are regularly placed along the compartment edges at an interval determined by their density per unit length, n_P (Fig. 1B). Using a recently developed multiscale simulation technique called BD-GFRD [6, 16–20] (see SI), we study the effect of confinement on the diffusion and the dimerization kinetics of S by varying n_C , n_P , and its number density per unit area, n_S and interaction between the molecules (Fig. 1C). We ask, how does confinement time depend on n_C and n_P ? Also, how does the dimerization rate depend on n_S and the interaction of the molecules?

Compartment hopping of a single molecule: To understand the diffusion of the particles in the presence of the pickets we studied the diffusion of a single tracer particle,

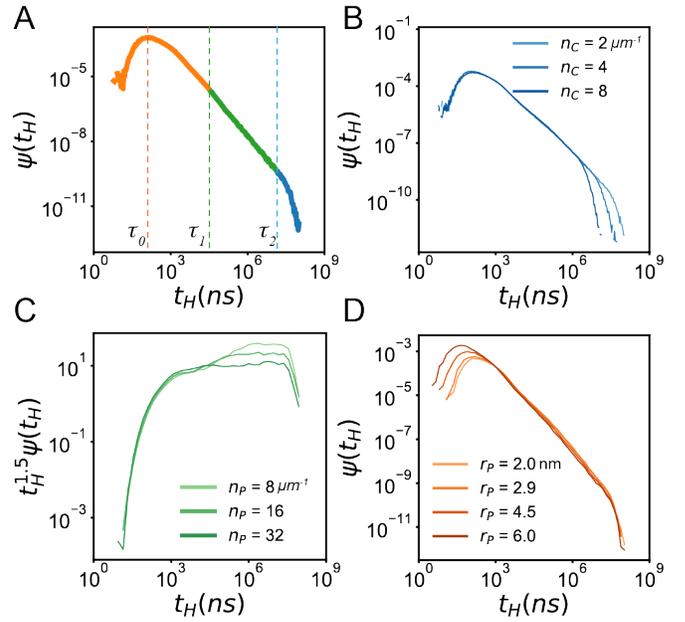


FIG. 2. Hopping time distribution: (A) Typical hopping time distribution observed for a single tracer particle diffusing on the compartmentalized membrane. Orange, green, and blue colors signify three phases of the hopping time distribution function $\psi(t_H)$. Blue denote exponential decay, which depends on the density of the compartments n_C (B). In green phase, the hopping time distribution decays as $\sim t_H^{-1.5}$ and the length of the green phase depend on n_P (C). Finally in the orange phase, hopping time distribution is non-monotonic and the position of the peak depends on r_P (D).

T . The immobile pickets along the compartment borders prevent T from escaping the compartment and the particle resides inside the compartment for time t_H , after which it “hops” to a neighboring compartment. The distribution of the hopping time, $\psi(t_H)$, is non-exponential at short times and exponential above a characteristic timescale, which implies that the hopping process is non-Markovian at short times and Markovian at long times (Fig. 2A). In addition, $\psi(t_H)$ shows at least three distinct phases: (1) Below a timescale τ_1 , $\psi(t_H)$ is non-monotonic with a peak at a timescale τ_0 and a power law tail that decays as $t_H^{-1.1}$; (2) Below τ_2 and above τ_1 $\psi(t_H)$ decays as $t_H^{-1.5}$; and (3) Above τ_2 , $\psi(t_H)$ decays exponentially. We found that each of these timescales depend on the system properties. τ_2 is determined by the compartment density n_C (Fig. 2B). The larger the compartment density, the smaller is the τ_2 . Similarly, the larger the picket density, n_P , the smaller is the timescale τ_1 (Fig. 2C). Finally, following the same trend, the larger the picket radius, the smaller is the timescale τ_0 (Fig. 2D). The dependence of these timescales on different densities as well as the picket radius implies that ultimately these densities and the picket radius controls one or more microscopic length scales that give rise to these characteristic timescales. Indeed, we find three such length scales

in our system. The compartment size, $L_c = n_C^{-1}$, determines the length scale $L_2 = L_c/2$. The particle T loses the memory of its initial condition if it has to diffuse for distance close to L_2 and the hopping time follows a poisson process with rate $\tau_2^{-1} = 4D/L_2^2$, where D is the diffusion coefficient of T . Similarly, τ_1 is determined by a length scale $L_1 = (n_P^{-1} - 2\sigma_{PT})/2$, where $\sigma_{PT} \propto (r_P + r_T)$ is a lengthscale determined by the radius of the pickets and the tracer particle. The proportionality constant is determined by the specific forms of interaction between the pickets and the tracer particles. For example, for LJ or WCA interactions, it is $2^{\frac{1}{6}}$. Finally, τ_0 is determined by a length scale $L_0 = L_{\text{sep}} - \sigma_{PT}$, where L_{sep} is distance between the picket center and the compartment boundary. If we assume that compartment boundary is determined by the actin fiber (7nm diameter [21]), then $L_{\text{sep}} = 3.5 \text{ nm} + r_P$ (Fig. S2). Although these lengthscales allow us to explain the three phases, they by themselves do not explain the behavior of $\psi(t_H)$ in each of these phases. To understand the hopping dynamics at each of these lengthscales, we measured the displacement during a hopping event. We found that around L_0 , the hopping time is determined by one dimensional first passage of the particles from one compartment to another. Around L_1 , the hopping time distribution is determined by first passage of the tracer through 2D diffusion. Finally, around L_2 , the hopping is a memoryless process and is determined by the Poisson process (Fig. S1). We can combine these three processes together, which generate a theoretical curve that reproduces the dependence of the hopping time distribution from the simulation (Fig. S3). More importantly, this characterization offers us a way to infer picket radius and density from experimental measurements of the residence times.

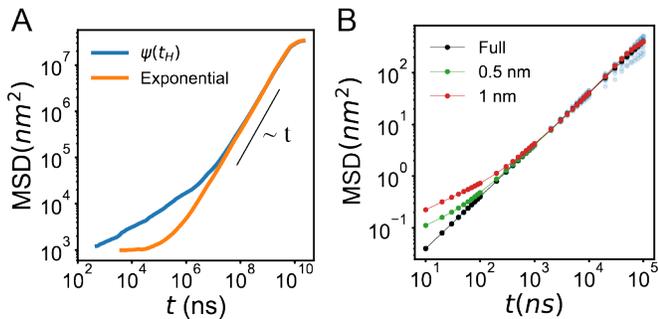


FIG. 3. **Diffusion of the tracer particle:** (A) Mean squared displacement (MSD) measured using a square lattice model (see text for details) shows anomalous diffusion for the hopping time distribution obtained from our simulation, whereas an exponential residence time distribution does not ($\text{MSD} \propto t$). (B) MSD calculated using BD suggests that diffusion of the tracer particle is not anomalous. However, if the BD trajectory is coarse-grained by placing grids of finite resolution (legend), then we observe anomalous diffusion.

Diffusion of the tracer particle: It is well-known that power law distributed residence times can give rise to anomalous diffusion [22–25]. Because the residence time distributions for the hopping particle decays as a power law for some timescales, we expected that at those timescales the particle will show anomalous diffusive behavior. To understand this process we measured the mean-squared displacement of the tracer particle by using Brownian Dynamics (BD) simulation and also by using a square lattice model. In the latter the transition times between two neighboring lattice points were randomly drawn from $\psi(t_H)$ and was compared with the case where transition times were drawn from an exponential distribution for which we observe normal diffusion (Fig. 3A). Much to our surprise, we found that mean squared displacement (MSD) computed using BD does not display any anomalous behavior (Fig. 3B), but the MSD computed from the lattice model does. This disagreement arises because in BD the displacement in a single step is proportional to the transition time, whereas for the lattice model the displacement is independent of the transition time. This observation suggests an intriguing possible origin of anomalous diffusion in experiments where the displacements cannot be resolved beyond the resolution of the microscopes. In such cases, the spatial transition are of constant length, but the timescale measured may not be commensurate with the resolution of the microscope. For example, for optical microscopes, the resolution is 200nm. For a lipid diffusing at $10 \mu\text{m}^2\text{s}^{-1}$, the average time required to explore 200 nm is approximately 4 ms. However, there are many experiments using optical microscopes that explore anomalous diffusion at μs regime [9, 10]. For such systems, the lack of spatial resolution may be another factor that may give rise to anomalous diffusion even when the diffusion is normal. To illustrate this point we took the trajectory of a particle undergoing normal diffusion and coarse-grained the spatial resolution while keeping the temporal resolution unchanged. We find that if the spatial resolution is l , then we get anomalous diffusion ($\text{MSD} \sim t^{0.5}$) up to a timescale $l^2/4D$ and for normal diffusion beyond this timescale (Fig. 3B).

Dimerization time distribution: We measure the dimerization time, t_D , using an ensemble in which we keep the number of monomer constant (SI). We find that beyond a timescale τ_{bulk} , the measured probability density function, $\psi_D(t_D)$, decays exponentially (Fig. 4 A). τ_{bulk} depends on the concentration of the monomers and is proportional to $n_S(n_S - 1)/2$, the WMMA flux. However, $\psi_D(t_D)$ deviates significantly from exponential distribution at times shorter than τ_{bulk} . Below a timescale $\tau_{2D}(n_S)$, $\psi_D(t_D)$ decays as t_D^{-1} , which we attribute to diffusion at short length-scales, where the collision between the monomers are not completely memoryless. In fact, the t_D^{-1} scaling originates from the time required to return to the reaction radius through 2D diffusion [3]. For

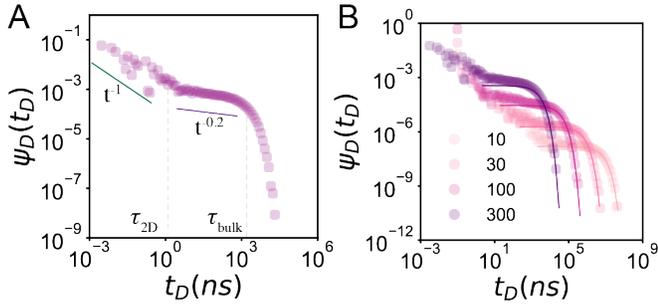


FIG. 4. **Dimerization time distribution** $\psi_D(t_D)$. (A) There are at least three phases in $\psi_D(t_D)$. At longest timescales ($t_D > \tau_{\text{bulk}}$), it decays exponentially and at shortest times ($t_D < \tau_{2D}$) it decays as t_D^{-1} . For intermediate timescales it decays as $t_D^{-0.2}$. (B) The size of the intermediate region is dependent on the density of the monomers n_S (legend). The dimerization rate at a given n_S is measured by fitting the tail of ψ_D with an exponential function (solid lines).

times between τ_{2D} and τ_{bulk} , $\psi_D(t_D)$ decays as $\sim t_D^{-0.2}$. We found that this scaling or the form of $\psi_D(t_D)$ does not depend on the density of the pickets for the densities explored in this paper. The physical processes underlying such uncommon scaling behavior remains unclear.

To measure the bulk dimerization rate, we fitted an exponential function to $\psi_D(t_D)$ for $t_D > \tau_{\text{bulk}}$. The PDF and the fitted exponential function is shown in Fig. 4. From these measured rates, we measured the dimerization “rate constant” $\kappa = \text{rate}/\phi$, where $\phi = n_S(n_S - 1)/2$, is the possible number of collisions between the n_S monomers. For WMMA kinetics to hold the collisions have to occur at a rate independent of the concentration of the molecules, so that κ should not depend on n_S . In the absence of any compartments, such that $n_P = 0$ or $n_C = 0$, we find that κ varies with n_S for all values of n_S . For $n_S < 10$, κ varies slowly with n_S , however, as $n_S = 10$ is approached from below, κ increases rapidly. For $n_S > 10$, κ increases algebraically with n_S . For $n_S < 100$, $\kappa \sim n_S^{0.25}$ and for $n_S > 100$, $\kappa \sim n_S^{0.5}$, with a discontinuity similar to $n_S = 10$ at $n_S = 100$. We also observe a similar trend in the variation of κ with n_S when the dimerization happens in compartmentalized membranes ($n_C > 0$ and $n_P > 0$). However, the absolute value of κ depends on the density of compartments n_C (Fig. 5A), but it does not depend on the density of the pickets (Fig. 5B). Dependence of κ on n_C , but not on n_P implies that the interaction of the tracer, with the pickets do not influence the diffusive collision rate. However, they influence the diffusive collision rates by confining the tracer within a compartment and denying free exploration of the entire membrane.

The intriguing variation of κ with n_S warrants a deeper investigation. The power law coefficient changes with increasing n_S because at low densities the interactions of

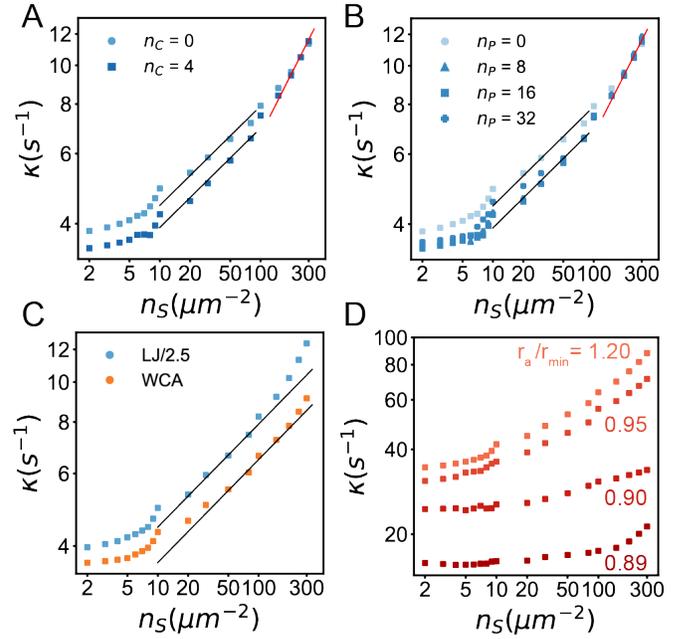


FIG. 5. **Reaction kinetics:** The “rate constant” κ is not a constant, but is a function of concentration. Its variation with n_S depends on n_C (A), but not on n_P (B). Also, there are at least three regions of variation for the n_S values investigated in this paper. (1) For $n_S < 10$, κ varies slowly with n_S , but it is not independent of n_S . (2) For $10 < n_S < 100$, $\kappa \sim n_S^{0.25}$ and (3) for $n_S > 100$, $\kappa \sim n_S^{0.5}$. (C) When κ is measured in the presence (LJ/2.5) and absence (WCA) of attractive interaction, the variations in region 1 and 2 are identical, but region 3 is absent for WCA. (D) The variation in region 1 and 2 is controlled by r_a . For $r_a < r_{\text{min}}$, we recover WMMA kinetics (see text). We used a diffusion constant of $10 \mu\text{m}^2/\text{s}$ for part (D), but it did not change the qualitative variation.

the monomers with each other do not influence the diffusion process, that is the drift term is too weak to influence the diffusion process. As n_S increases, the drift term becomes more important and we start seeing its influence on the diffusive collision rates. Confirming this hypothesis analytically is difficult due to the complex boundary conditions associated with this problem. However, we note that this hypothesis can be tested easily by comparing the diffusive collision rates in the presence and absence of attractive interactions, If the change in power law is investigated by particle-particle interactions, then we should expect to observe different power law exponents for attractive and repulsive interactions. This is indeed what we find. As Fig. 5C shows, for attractive LJ interaction (Fig. 1C), the power law changes at $n_S \sim 100$, but for the excluded volume WCA [26] interactions, the power law does not change within the investigated values of n_S and it varies as $n_S^{0.25}$. We should point out that the association reactions happened in both of these cases as soon two particles come closer than the association reaction radius $r_a = 1.2 r_{\text{min}}$, where $r_{\text{min}} = 2^{1/6}\sigma$ is the distance

at which the particles start to feel the repulsion due to excluded volume interaction. Therefore, perhaps the $n_S^{0.25}$ variation may be explained by calculating the probability of finding two particles within a prescribed distance. We found that for any $\frac{r_a}{r_{\min}} \geq 1$, we observe similar scaling, which consolidates our conjecture about the origin of the $n_S^{0.25}$ scaling. Conversely, if this statement is indeed true then reducing r_a below r_{\min} should change this scaling. This is indeed what we find (Fig. 5D). As r_a is reduced, not only does κ at constant n_S decrease, its variation with n_S also changes. For $r_a = 0.89r_{\min}$, the scaling exponent is approximately zero for $n_S < 100$, so that κ varies slowly with n_S . For such slow variations, the violation of WMMA approximation is minimal. This is expected because for $r_a = 0.89r_{\min}$, many collisions are required before the monomers can form a dimer, which reduces k_I well below k_D , so that the WM criterion is satisfied. Furthermore, the interaction is effectively hard sphere collision at such small distances, so that MA condition is also satisfied. So, in principle it is possible to apply WMMA approximation to model biomolecular reactions. However, we note that biomolecular reactions have evolved in such a way that reactions happen almost immediately after a collision [6, 21]. So, in practice, WMMA kinetics is not an appropriate choice for biomolecular reactions.

We have investigated the kinetics of dimerization reaction in a simple model of biological membrane. In that context we have presented definite proof against the applicability of WMMA kinetics for biomolecular reactions. Moreover, we have found that the variation of dimerization rate with monomer concentration does not depend on the picket density and is modulated only by the interaction between the monomers. However, the immobility of the pickets may have led to the observed independence. The pickets may weakly diffuse along the actin fence, which may influence the diffusive transport of the monomers, which we will explore in a future paper. Even in the absence of such complexity, our model offers an elegant way to explore biomolecular kinetics and gives definite shape and form to the nebulous idea that WMMA kinetics is not appropriate for biomolecular kinetics. We anticipate our approach will inspire new investigations into biomolecular reaction kinetics and reveal the laws that govern processes inside a cell.

This work was funded by an LDRD grant (XX01) from LANL and has the following LA-UR number: LA-UR-20-20267. The author thanks Prof. Angel E. Garcia and Dr. Van A. Ngo for useful discussion and Prof. Yair Shokef and Dr. Sumit Majumder for critical reading of the manuscript.

- [1] P. Atkins, J. de Paula, and J. Keeler, *Atkins' Physical Chemistry 11e* (Oxford University Press, Oxford, United Kingdom ; New York, NY, 2018), 11th ed., ISBN 978-0-19-876986-6.
- [2] M. O. Vlad, A. D. Corlan, F. Morán, R. Spang, P. Oefner, and J. Ross, PNAS **106**, 6465 (2009), ISSN 0027-8424, 1091-6490.
- [3] K. Takahashi, S. Tanase-Nicola, and P. R. ten Wolde, Proc. Natl. Acad. Sci. U.S.A. **107**, 2473 (2010), ISSN 1091-6490.
- [4] M. Dibak, C. Fröhner, F. Noé, and F. Höfling, J. Chem. Phys. **151**, 164105 (2019), ISSN 0021-9606.
- [5] H. Berg and E. Purcell, Biophysical Journal **20**, 193 (1977), ISSN 00063495.
- [6] S. Sarkar and A. E. Garcia, bioRxiv 810150 (2019).
- [7] M. C. Cross and P. C. Hohenberg, Rev. Mod. Phys. **65**, 851 (1993).
- [8] A. M. Turing, Philosophical Transactions of the Royal Society of London. Series B, Biological Sciences **237**, 37 (1952).
- [9] A. Kusumi, K. G. N. Suzuki, R. S. Kasai, K. Ritchie, and T. K. Fujiwara, Trends in Biochemical Sciences **36**, 604 (2011), ISSN 0968-0004.
- [10] A. Kusumi, C. Nakada, K. Ritchie, K. Murase, K. Suzuki, H. Murakoshi, R. S. Kasai, J. Kondo, and T. Fujiwara, Annu. Rev. Biophys. Biomol. Struct. **34**, 351 (2005), ISSN 1056-8700.
- [11] A. Kusumi, T. K. Fujiwara, N. Morone, K. J. Yoshida, R. Chadda, M. Xie, R. S. Kasai, and K. G. N. Suzuki, Seminars in Cell & Developmental Biology **23**, 126 (2012), ISSN 1084-9521.
- [12] S. Sadegh, J. L. Higgins, P. C. Mannion, M. M. Tamkun, and D. Krapf, Phys. Rev. X **7**, 011031 (2017).
- [13] D. Krapf, Current Opinion in Cell Biology **53**, 15 (2018), ISSN 0955-0674.
- [14] Z. Kalay, T. K. Fujiwara, and A. Kusumi, PLOS ONE **7**, e32948 (2012), ISSN 1932-6203.
- [15] B. J. Sung and A. Yethiraj, Biophysical Journal **97**, 472 (2009), ISSN 0006-3495.
- [16] A. Vijaykumar, P. G. Bolhuis, and P. R. ten Wolde, J. Chem. Phys. **143**, 214102 (2015), ISSN 0021-9606.
- [17] A. Vijaykumar, T. E. Ouldridge, P. R. Ten Wolde, and P. G. Bolhuis, J Chem Phys **146**, 114106 (2017), ISSN 1089-7690.
- [18] T. R. Sokolowski, J. Pajmans, L. Bossen, T. Miedema, M. Wehrens, N. B. Becker, K. Kaizu, K. Takahashi, M. Dogterom, and P. R. ten Wolde, J. Chem. Phys. **150**, 054108 (2019), ISSN 0021-9606.
- [19] L. Sbailò and F. Noé, J Chem Phys **147**, 184106 (2017), ISSN 1089-7690.
- [20] V. A. Ngo, S. Sarkar, C. Neale, and A. E. Garcia, Manuscript available upon request. (2019).
- [21] B. Alberts, A. D. Johnson, J. Lewis, D. Morgan, M. Raff, K. Roberts, and P. Walter, *Molecular Biology of the Cell* (W. W. Norton & Company, New York, NY, 2014), sixth edition ed., ISBN 978-0-8153-4432-2.
- [22] J.-P. Bouchaud and A. Georges, Physics Reports **195**, 127 (1990), ISSN 0370-1573.
- [23] R. Metzler and J. Klafter, Physics Reports **339**, 1 (2000), ISSN 0370-1573.
- [24] S. Havlin and D. Ben-Avraham, Advances in Physics **51**,

187 (2002), ISSN 0001-8732.

- [25] D. Krapf, in *Current Topics in Membranes*, edited by A. K. Kenworthy (Academic Press, 2015), vol. 75 of *Lipid Domains*, pp. 167–207.
- [26] J. D. Weeks, D. Chandler, and H. C. Andersen, *J. Chem. Phys.* **54**, 5237 (1971), ISSN 0021-9606.

SUPPLEMENTARY INFORMATION

METHODS

Green’s function reaction dynamics (GFRD)

The challenge to studying the dimerization reactions at biologically relevant concentrations of the molecules lies in the fact that biological dynamics occur over multiple timescales. For example, as we mentioned before, the timescale for diffusive collision is at least three orders of magnitude larger than the reaction timescales. Such disparate timescales are difficult to handle using traditional molecular simulation techniques. To circumvent this constraint, we employ a recently developed multiscale simulation technique called Green’s function reaction dynamics or GFRD. To understand how GFRD works, note that biomolecular systems are sparse and biomolecular interactions are short-ranged. Therefore, in biomolecular simulations, most of the computational resources is spent on propagating the particles towards each other through diffusion. Because interactions are short-ranged, the molecules remain isolated from the influence of other molecules and perform free diffusion. Leveraging this fact, GFRD computes the space available to a molecule for free diffusion and measures the time required to traverse this space diffusively using the Green’s function appropriate for the boundary condition. Once the molecules reach the interaction distance, the algorithm switches to traditional molecular mechanics algorithms, e.g. Brownian Dynamics in this paper. Thus, by switching between the event driven and the molecular mechanics algorithms, Brownian Dynamics - GFRD (BD-GFRD) achieves almost a million-fold speed up compared to just Brownian Dynamics algorithm. Therefore, with similar computational resources, BD-GFRD can explore systems with dynamics spanning picoseconds to seconds timescale.

Simulation details

We performed all simulations on a two-dimensional $1 \mu\text{m} \times 1 \mu\text{m}$ simulation box with periodic boundary condition. Unless otherwise stated, the monomers, S , interacted with each other through attractive Lennard-Jones interaction (Fig. 1C) with interaction strength $\epsilon = 5kT$, and cutoff radius $r_c = 2.5\sigma$, where $\sigma = r_i + r_j$ is the

sum of the radius of the two interacting particles. The pickets interacted with other pickets and the monomers with WCA interaction (Fig. 1C) of strength $\epsilon = 5kT$. A single monomer was chosen as the tracer particle. Hence its interaction with the pickets excluded volume WCA interaction. The diffusion coefficient of the monomers was $D = 1\mu\text{m}^2/s$ except for Fig. 5D, where the diffusion coefficient was $10\mu\text{m}^2/s$. The change in diffusion coefficient did not change the kinetics qualitatively.

Studying dimerization reaction using BD-GFRD

In this letter, we use BD-GFRD to study the dimerization kinetics spanning 10 orders of magnitude in timescales. To measure dimerization rates from BD-GFRD simulations, we used an ensemble in which the number of monomers were kept constant. To do so, as soon as two monomers formed a dimer, the dimer was removed from the simulation box and was replaced by two monomers that were placed at random locations. We ran the simulation for up to 10 seconds simulation time or 96 CPU-hours, whichever was shorter, which generated on an average about 10^4 dimerization events for each parameter sets. Using these data, we constructed histograms of dimerization and fitted the tails of the histograms with an exponential function to estimate the dimerization rates.

Hop diffusion using BD-GFRD

We measure the hopping time, t_H using BD-GFRD. To do so, we study the diffusion of a single tracer particle on the compartmentalized membrane. The compartment coordinates are stored in a look-up table. After each position update, using the look-up table we check whether the tracer particle has changed compartment or not. If it has, then we store the time and location of the hop in a file. When doing analysis of the hopping time, we measure the inter-hop time and construct a histogram using logarithmically spaced bin edges. The number of bins in the histogram has been chosen according to the following formula:

$$n_{bin} = 2n^{2/5}, \quad (4)$$

where n is the total number of samples. It can be shown that for variable bin widths, as is the case when bin edges are chosen logarithmically, this formula generates equiprobable bins. Using BD-GFRD, we generated at least 10^5 data points. Accordingly, we had created the histograms using ~ 200 bins.

We have also computed the hopping time distribution using only Brownian Dynamics (BD) simulation. The hopping time distribution obtained using BD matches with the distribution obtained using BD-GFRD.

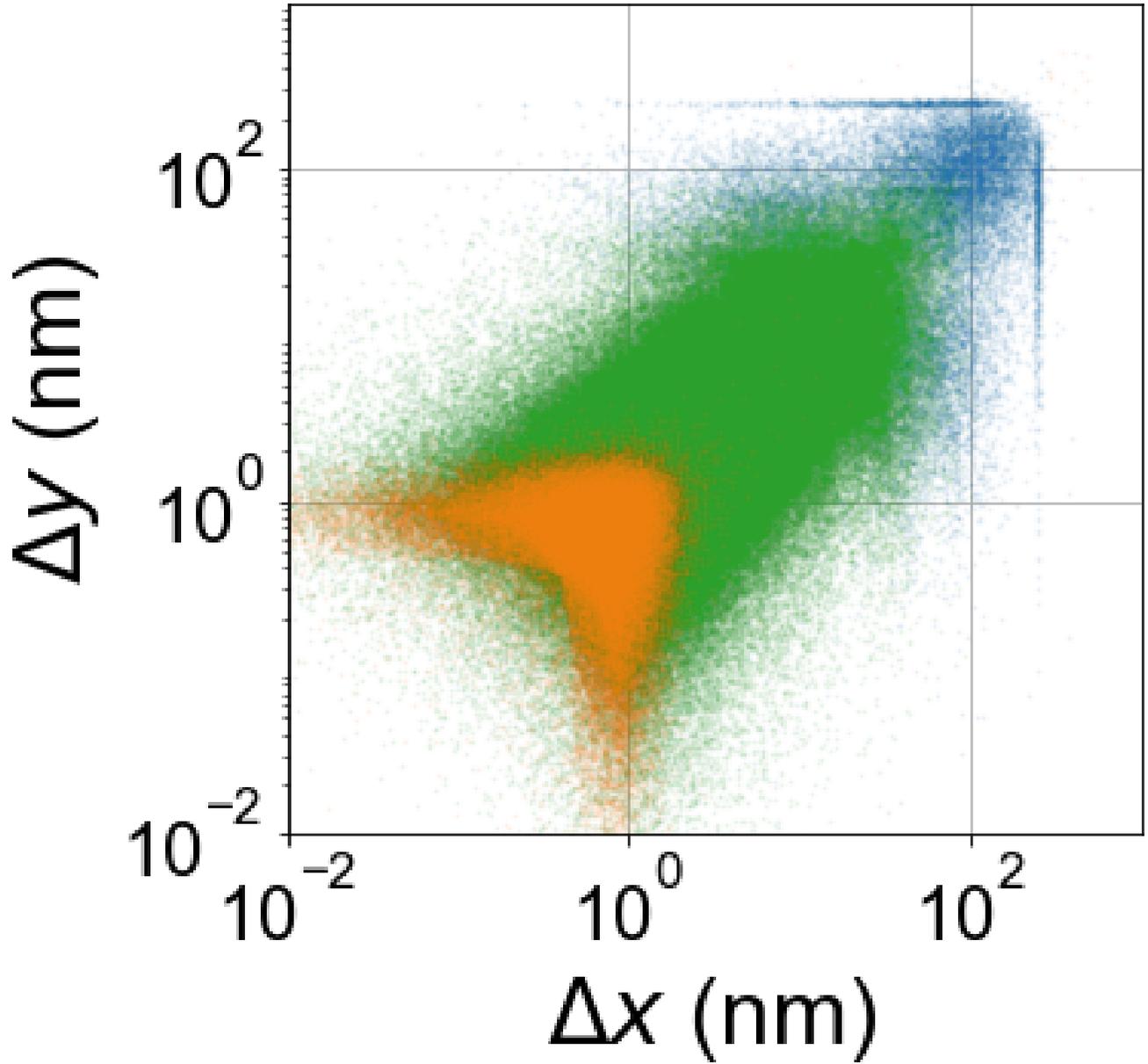


FIG. S1. Displacements of the tracer particles while hopping at different timescales. For $t_H < \tau_0$ (orange), the displacements are quasi-1D . Therefore, the hopping time is determined by 1D first passage process. For $\tau_1 < t_H < \tau_2$ (green), the displacements are two dimensional, but at small spatial scales. So, the hopping time is determined by 2D first passage process. For $t_H > \tau_2$ (blue), the displacements are 2D and at large spatial scales. Therefore, the hopping process loses the memory of its initial condition and the hopping time is determined by a poisson process.

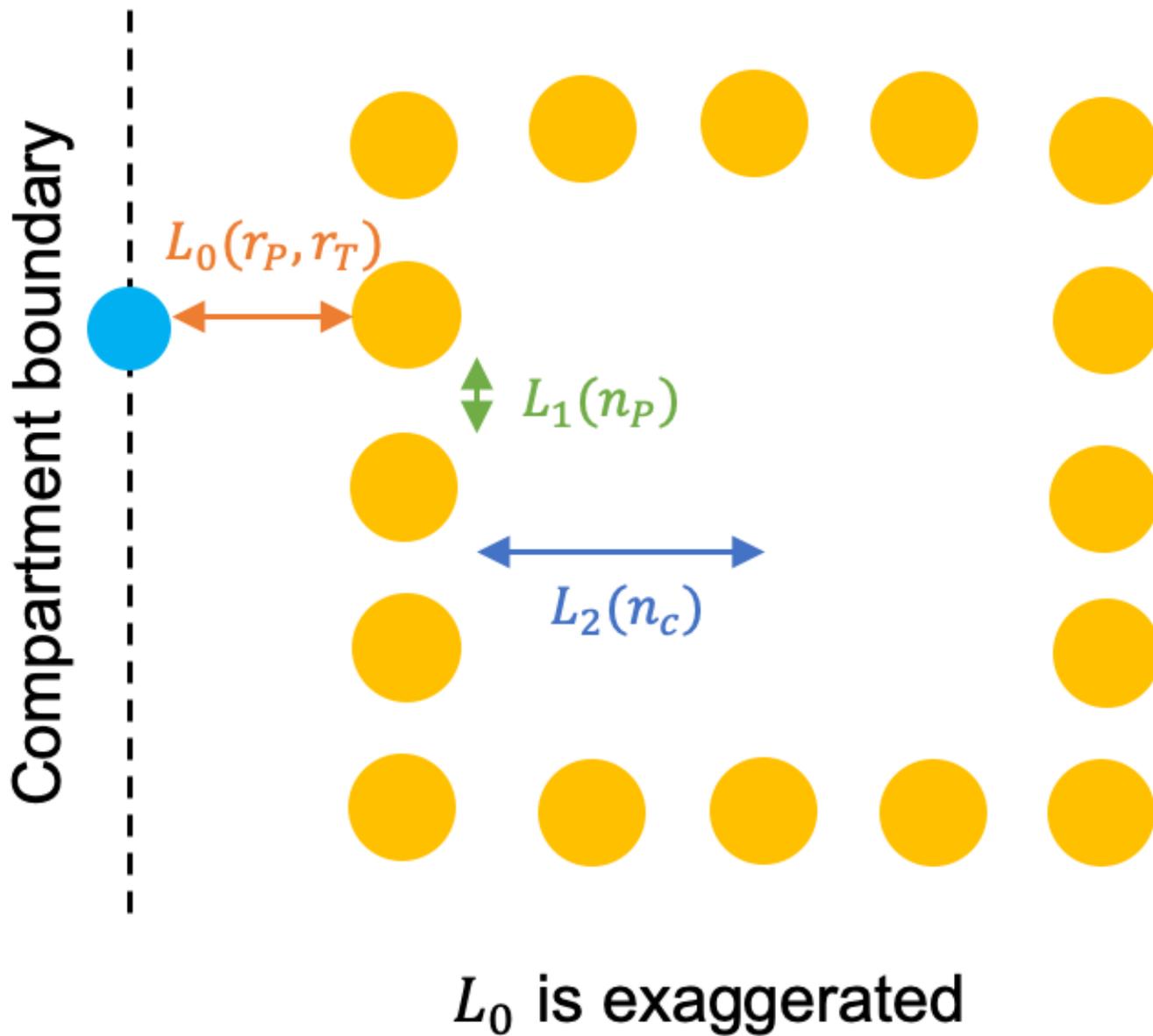


FIG. S2. Illustration of different hopping length scales. None of the length scales are shown to scale and L_0 is exaggerated.

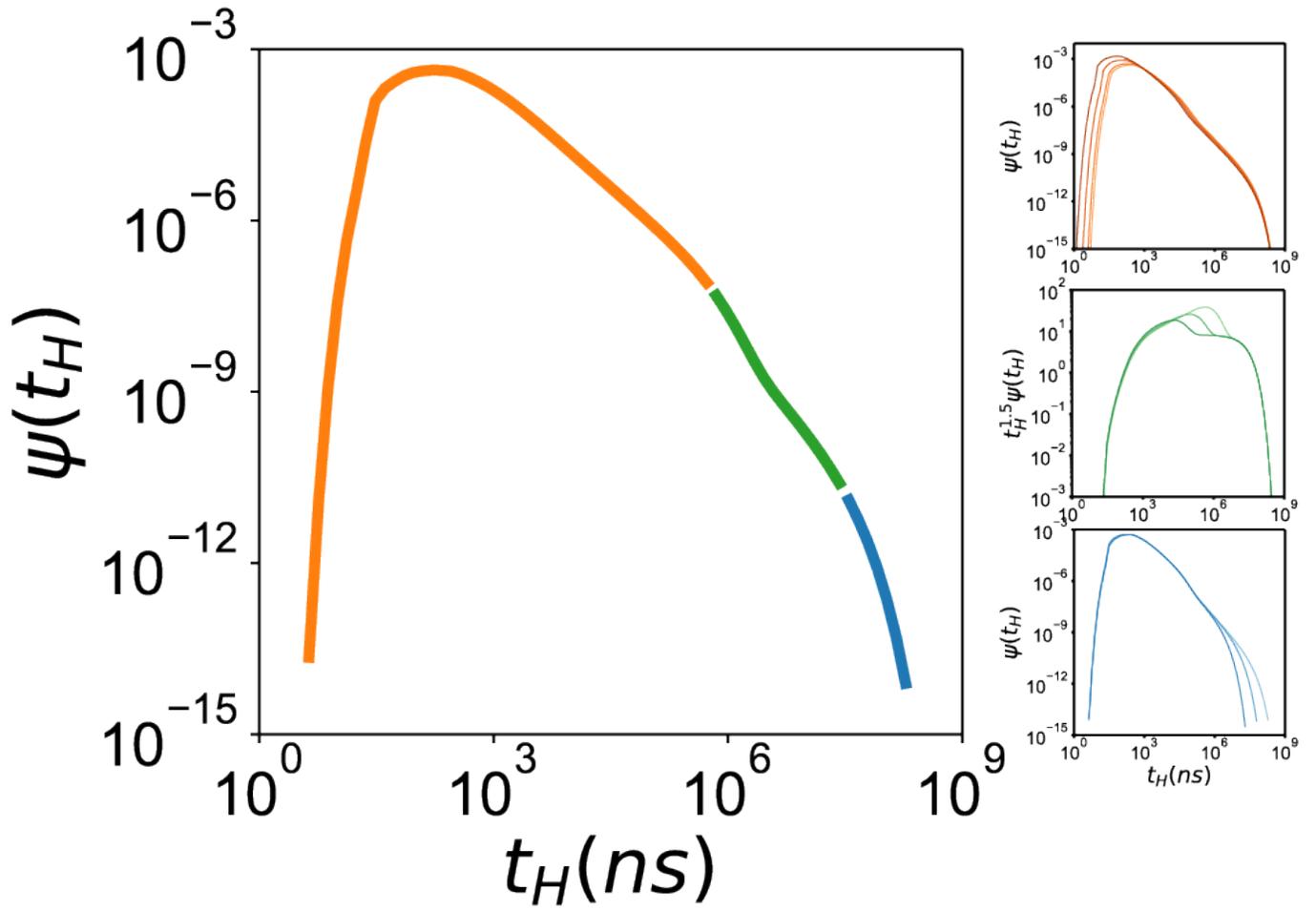


FIG. S3. Hopping time distribution obtained from analytical calculation shows the same three phases as obtained from the simulation (Fig. 2).